

# Quantum tunneling dynamics using hydrodynamic trajectories.

Eric R. Bittner

*Department of Chemistry, University of Houston, Houston, TX 77204*

(Submitted to J. Chem. Phys.)

In this paper we compute quantum trajectories arising from Bohm's causal description of quantum mechanics. Our computational methodology is based upon a finite-element moving least-squares method (MWLS) presented recently by Wyatt and co-workers (Lopreore and Wyatt, Phys. Rev. Lett. **82**, 5190 (1999)). This method treats the "particles" in the quantum Hamilton-Jacobi equation as Lagrangian fluid elements which carry the phase,  $S$ , and density,  $\rho$ , required to reconstruct the quantum wavefunctions. Here, we compare results obtained via the MWLS procedure to exact results obtained either analytically or by numerical solution of the time dependent Schrödinger equation. Two systems are considered: firstly, dynamics in a harmonic well and secondly tunneling dynamics in a double well potential. In the case of tunneling in the double well potential, the quantum potential acts to lower the barrier separating the right and left hand sides of the well permitting trajectories to pass from one side to another. However, as probability density passes from one side to the other, the effective barrier begins to rise and eventually will segregate trajectories in one side from the other. We note that the MWLS trajectories exhibited long time stability in the purely harmonic cases. However, this stability was not evident in the barrier crossing dynamics. Comparisons to exact trajectories obtained via wave packet calculations indicate that the MWLS trajectories tend to underestimate the effects of constructive and destructive interference effects.

## I. INTRODUCTION

Trajectory based constructions of quantum behavior are ubiquitous throughout quantum physics. In the semi-classical limit, quantum dynamics is approximated by classical equations of motion whereby the transition amplitudes and wavefunctions are computed using the classical action connecting the initial and final states. Hydrodynamic constructions date back to early work by de Broglie<sup>1-5</sup> and Madelung<sup>7</sup> later by Bohm.<sup>7,8</sup> The so called quantum trajectories arising from this formalism have been the subject of a large number of ontological and philosophical papers seeking a causal interpretation of quantum mechanics. While a comprehensive overview of these works is far beyond the scope of this paper, Holland's book provides perhaps the most comprehensive technical overview of the approach and contains many examples of how the formalism can be applied in a wide variety of cases.<sup>9</sup> In short, the quantum trajectories themselves are relatively easy to compute once one has obtained a wavefunction solution of Schrödinger equation,  $\psi$ . The velocity of a trajectory at a given point in space-time is computed as

$$v(x, t) = \frac{j(x, t)}{\rho(x, t)} \quad (1)$$

where  $j(x, t)$  is the quantum current, and  $\rho = |\psi|^2$ . In this "pilot wave" approach,  $\psi$  acts as a guiding field for the trajectories. This approach is useful in that once the wave function has been obtained, is generally easy to compute the trajectories. While there are a number of papers which have computed quantum trajectories having obtained the wave function, relatively little work has been done in developing computational methods based upon the description which does not rely upon first constructing the wave function.<sup>10-15</sup> However, Wyatt and co-workers have recently described a mesh-less finite-element method for integrating the de Broglie-Bohm equations using Lagrangian hydrodynamic trajectories.<sup>16-18</sup> Similar methods are widely used in computational fluid dynamics (CFD) to simulate fluid flow dynamics in porous media (such as an oil reservoir) and other systems with complex topologies.<sup>20</sup> Wyatt's method represents the quantum density using a cloud of Lagrangian fluid points which themselves evolve according to the de Broglie-Bohm hydrodynamic equations of motion. The method features a moving weighted least-squares (MWLS) approach to compute the various derivatives and gradients required by the de Broglie-Bohm equations.

In this work, we report on our implementation of the MWLS methodology and present an assessment of its difficulties and where improvements can be made. Previous applications of the approach have focused entirely upon reactive scattering type calculations. While this class of problems has its own set of associated difficulties, we have elected to focus upon the dynamics of systems trapped in various one dimensional potential wells. These problems, while perhaps too idealistic, allow one to compare trajectories and results obtained via a "hydrodynamic" calculation to those obtained via analytical or numerical solution of the time-dependent Schrodinger equation. Specifically, we first examine the dynamics of harmonic oscillators and then move onto a more challenging problem of tunneling in double well potential. Our results indicate that the methodology reproduces results obtained via more traditional grid based

approaches; however, we note that the long time stability of the methodology needs to be improved before it can be used as an alternative to wave-packet based calculation.

## II. QUANTUM EQUATIONS OF MOTION

The de Broglie-Bohm equations are derived directly from the time dependent Schrödinger equation. The derivation is initialized by writing the wave function in polar form:

$$\psi(x, t) = R(x, t)e^{iS(x, t)/\hbar}. \quad (2)$$

When this substituted into the Schrödinger equation, the real and imaginary components can be collected into a continuity equation:

$$\partial_t \rho(x, t) + \frac{1}{m} \nabla \cdot (\rho \nabla S) = \quad (3)$$

and the quantum Hamilton-Jacobi equation:

$$\partial_t S + \frac{|\nabla S|^2}{2m} + V + Q = 0 \quad (4)$$

where  $Q$  is the so called quantum potential which is non-local and arises from the quantum kinetic energy operator in the Schrödinger equation.

$$Q(x, t) = -\frac{\hbar^2}{2m} \frac{1}{\sqrt{\rho}} \nabla^2 \sqrt{\rho} \quad (5)$$

Taking the gradient of Eq.4, one obtains the equations of motion for the trajectories:

$$D_t v(x, t) = -\frac{1}{m} \nabla (V(x(t)) + Q(x(t))) \quad (6)$$

where we define  $x(t)$  and  $v(x(t)) = \nabla S/m$  as the trajectory and velocity of Lagrangian fluid elements. The notation  $D_t f$  denotes the “material” or “convective” derivative of the function  $f$

$$D_t f = (\partial_t + v \cdot \nabla) f \quad (7)$$

which gives the rate of change of  $f(x(t))$  as observed while moving with the particle along the trajectory,  $x(t)$ .<sup>22,23</sup> Hence in the Lagrangian picture of fluid mechanics, we “go with the flow”. The equation of continuity can also be written in terms of the convective derivative:

$$D_t \rho + (\nabla \cdot v) \rho = 0 \quad (8)$$

From this we can deduce a short time propagator for  $\rho$ :

$$\rho(x, t + \delta t) = e^{-\nabla \cdot v \delta t} \rho(x, t) \quad (9)$$

which is local in space and is dependent upon the divergence of the velocity field at the point  $x$ . To apply Eq. 6 and Eq. 9 in a computational scheme, we first discretize the system into an ensemble of Lagrangian fluid elements labeled by their position vectors,  $x$ . These elements carry information regarding the local density about that point and the phase is determined by integrating Eq. 5 along the path. From these two bits of information, the quantum wavefunction can be reconstructed by writing<sup>18</sup>

$$\psi(x_i, t) = \sqrt{\rho(x_i, 0)} \exp \left( \frac{i}{\hbar} \int_0^t L(x_i, v_i, \tau) d\tau + \frac{i}{\hbar} S(x, 0) \right) \exp \left( -\frac{1}{2} \int_0^t \nabla \cdot v(\tau) d\tau \right) \quad (10)$$

where

$$L(x, v, t) = \frac{1}{2} m v^2 - V - Q \quad (11)$$

is the quantum Lagrangian and  $S(x, 0)$  represents any initial spatial dependent phase present in the initial wave function, such as  $S(x, 0) = \hbar kx$ .

In order to compute expectation values we need to be able to integrate over the spatial domain spanned by either  $\rho$  or  $\psi$ . If we require that each trajectory element carry a volume element,  $dx(t)$ , then by normalization

$$1 = \int dx(0) \rho(x, 0) = \sum_{i=1}^N \rho_i(0) dx_i(0) = \sum_{i=1}^N \rho_i(t) dx_i(t), \quad (12)$$

where  $\rho_i(t) = \rho(x_i(t))$  is the density carried by the  $i$ th trajectory.

To compute  $dx_i(t)$  we need the Jacobian which transforms the volume element  $dx_i(0)$  to the volume element,  $dx_i(t)$  some time later along trajectory  $x_i(t)$ .

$$J_i = \frac{\partial x_i(0)}{\partial x_i(t)}. \quad (13)$$

Taking the material time derivative of  $J$  yields along each trajectory:

$$D_t \log J_i = \nabla \cdot v_i \quad (14)$$

Thus, an amplitude element of the wavefunction is propagated along a trajectory  $x_i(t)$  as

$$\begin{aligned} dx_i(t) \psi_i(t) &= dx_i(0) \sqrt{\rho_i(0)} \exp \left( \frac{i}{\hbar} \int_0^t L(x_i, \dot{x}_i, \tau) d\tau + \frac{i}{\hbar} S(x_i, 0) \right) \\ &\times \exp \left( - \int_0^t \nabla \cdot v_i(\tau) d\tau \right). \end{aligned} \quad (15)$$

A typical propagation cycle consists of computing the quantum potential from the density at each fluid element, taking the gradient of  $Q$  and  $V$  to compute the acceleration of the fluid element and computing divergence of the velocity field to determine how the density in given fluid element changes over one discrete time interval. Thus, the trajectories, density, and velocity fields contain all of the essential information required to construct the full quantum mechanical wave function.

### III. MOVING LEAST SQUARES APPROXIMATION

Since our goal is to be able to compute the quantum trajectories without computing the wavefunction *a priori*, we need to be able to discretize the system into a set of Lagrangian fluid elements, compute the various derivatives required to compute the equations of motion and finally, advance the fluid elements to a new set of coordinates. This we accomplish through the use of an adaptive meshless-cloud method described recently by Wyatt<sup>16–18</sup>. The method itself is described in detail by Liszka and co-workers<sup>20</sup> and is similar to methods used extensively in computational fluid dynamics. First, we review the finite element approximation<sup>21</sup> (FEA) and its implementation in a movable weighted least-squares scheme (MWLS).

In the moving least squares approximation, we assume that we have a function,  $g = g(x)$  defined over a finite set of points and we seek an approximate value of  $g$  at one of these points,  $x_o$ , based upon the values at neighboring points. We assume that the function we seek is smooth enough to be expanded about the point  $x_o$  in a finite polynomial basis

$$p = \left\{ x, \frac{x^2}{2}, \dots, \frac{x^{n_p}}{n_p!}, \right\} \quad (16)$$

Thus, we can write

$$f(x) = \sum_{i=1}^{n_p} a_i p_i(x - x_o) + f(x_o) \quad (17)$$

where  $a_i$  is a vector of coefficients. For a simple polynomial as above, the derivatives of  $f$  at  $x_o$  are then just the coefficients themselves. If we have a data point at  $x_o$  and we want the approximation to pass through the remaining data points, we can write a set of least-squares equations

$$f_j = \sum_{i=1}^{n_p} a_i p_i(x_j - x_o), \quad (18)$$

where  $f_j = f(x_j) - f(x_o)$ ,  $p_i(x_j - x_o)$  is the  $i$ th polynomial basis member evaluated at  $x_j - x_o$ , and  $a_i$  are the expansion coefficients. In other words, we seek a vector  $a$  which satisfies the linear equation:

$$f = P \cdot a \quad (19)$$

where  $f$ ,  $P$ , and  $a$  are the terms in Eq. 18 written in matrix/vector form.

In order to solve for  $a$ , we need at least as many data points in the neighborhood about  $x_o$  as we have terms in the polynomial expansion. Rather than trying to pick out exactly the right number of points, the most efficient procedure is to simply select more data points than basis functions. Since the system of equations is overdetermined,  $P$ , is a rectangular matrix and we use must either singular value decomposition or other pseudo-inversion method to invert  $P$ . Furthermore, we can improve the stability of the least squares procedure by weighting each data point so that points farther away from the central point receive the least weight. Thus, for the "weighted" least squares procedure we solve

$$f^\Omega = P^\Omega \cdot a \quad (20)$$

where  $f_j^\Omega = (f_j - f(x_o))\omega_j$ ,  $P_{ij}^\Omega = \omega_j P_{ij}$ ,  $a$  is a vector of undetermined coefficients, and  $\omega_j$  is the weight assigned to point  $x_j$ .

We have found that the convergence of the least-squares procedure is greatly improved by using a logarithmic form of the density<sup>15,17,19</sup>,

$$\rho = e^{g(x)}, \quad (21)$$

where  $g$  is a polynomial of order  $n_p$ . This representation is a useful way to transform a non-linear model to a linear one. For example, in computing the quantum potential we can write

$$\frac{1}{\sqrt{\rho}} \nabla^2 \sqrt{\rho} = e^{-g/2} \nabla^2 e^{g/2} \quad (22)$$

Working through the derivative terms yields:

$$e^{-g/2} \nabla^2 e^{g/2} = \frac{1}{2} \left( g_{,\mu\mu} + \frac{1}{2} g_{,\mu}^2 \right) \quad (23)$$

where the "comma" delimited subscripts in  $g_{,u} = \partial_\mu g$  denote taking derivative with respect to coordinate  $\mu$ .

Finally we write the equations of motion for the velocity in terms of the derivatives of the various fields in component form:

$$ma_\mu(x) = -\partial_\mu \left( V(x) - \frac{\hbar^2}{4m} \left( g_{,\nu\nu} + \frac{1}{2} g_{,\nu}^2 \right) \right) \quad (24)$$

$$\rho(x, t + \delta t) = e^{-\partial_\mu v_\mu(x) \delta t} \rho(x, t). \quad (25)$$

Some final notes regarding our implementation of the MWLS scheme are also in order. We propagate trajectories using the symplectic Verlet algorithm<sup>24</sup>. Convergence with respect to time step is checked by comparing the results of two 1/2 time steps to one full time step. If the differences between position, energy, velocity, or  $\rho$  computed via the two separate procedures varied by more than  $1 : 10^6$ , the shorter time step results were taken,  $\delta t$  was reduced by a factor of 0.75 and propagation continued. However, if the longer time step results were sufficiently accurate,  $\delta t$  was increased by a factor of 2 for the next iteration cycle. For the least squares fitting procedures, we found that a Hermite polynomial basis provided the most robust basis as measured by the  $\chi^2$  for each fit. We also weighted the fits using a Gaussian weighting function centered about  $x_o$  adjusted so that the point farthest from  $x_o$  received a weight of 0.01. For the one dimensional results presented here, our code reproduces results obtained via Wyatt's MWLS particle code described in Ref.<sup>16</sup>

## IV. EXAMPLE CALCULATIONS

### A. Harmonic Oscillator

As a primary example, we consider the quantum trajectories for a harmonic oscillator and compare these to the classical trajectories starting from identical starting points. In Fig. 1 we show the time evolution of an ensemble of quantum trajectories for a harmonic system with period of  $\tau = 2\pi/\omega = 888.57a.u.$  Unless otherwise noted explicitly, we shall use atomic units from here on, setting  $\hbar = 1$ . The first two cases (A & B) are the quantum trajectories for a particle with mass  $m = 2000a.u$  and with mass  $m = 200a.u.$  respectively, each starting with identical initial quantum densities

$$\rho(x) = e^{-\beta(x-x_o)^2} \quad (26)$$

with  $x_o = 3.0$  and  $\beta = 0.3$ .

In each of the cases shown here, we used 100 points spaced evenly about the center of the initial density. In fourth plot (D) we show the trajectories obtain from a purely classical calculation involving the same 100 points. The effect of the quantum potential is clearly seen as the trajectories traverse the minimum of the well at  $x = 0$ . For the heavier mass (in A), the trajectories tend to focus at the well minimum, just as in the classical calculation (in D). However, the trajectories *do not cross* each other as do the classical trajectories. This is a crucial characteristic of Bohmian trajectories. In essence, the density must be single valued and the Jacobian of the volume element carried by each point must remain positive definite for all times. Hence, if any pair of trajectories were to cross, these conditions would be violated. For case B, in which  $m = 200a.u$ , the quantum potential is  $10\times$  stronger than in case A and hence the trajectories become more diffuse as the particle traverses the bottom of the well. Interestingly enough, if we instead choose  $\beta = 1/m\omega$ , the trajectory lines remain evenly spaced throughout the calculation as shown in C.

This last result can be understood from the fact that the wavepacket used in Fig. 1.C is a coherent state and hence the time evolution of the density is given by

$$\rho(x, t) = e^{-m\omega(x-x_o \cos(\omega t))^2} \quad (27)$$

where  $x_o$  is the original centroid of the wavepacket. The quantum potential can be easily derived from Eq. 26 and the action along any given Bohmian trajectory is given by<sup>9</sup>

$$S(x, t) = \frac{1}{2}\hbar\omega t - \frac{1}{2}m\omega \left( 2xx_o \sin(\omega t) - \frac{1}{2}x_o^2 \sin(2\omega t) \right). \quad (28)$$

Thus, each trajectory is a solution of

$$m\dot{x} = \partial_x S = -m\omega x_o \sin \omega t. \quad (29)$$

and belongs to the family of cosine curves of period  $\omega$ :

$$x_i(t) = x_i(0) + x_o(\cos(\omega t) - 1). \quad (30)$$

*I.e.* the Bohmian particle undergoes simple harmonic motion of amplitude  $x_o$  about the point  $x_i(0) - x_o$ . Furthermore, the energy along a given Bohmian trajectory is computed by taking the time derivative of the action (Eq. 28):

$$E(x, t) = \partial_t S = \frac{\hbar\omega}{2} - \frac{1}{2}m\omega^2(2xx_o \cos(t\omega) - x_o^2 \cos(2t\omega)). \quad (31)$$

Note that this is not constant in time as would be expected for a purely classical system. The quantum force thus acts as a time dependent driving force on the ensemble of trajectories. If we were to have chosen the initial center of the density to be at exactly  $x = 0$ , then  $E = \hbar\omega/2$  and the quantum force would exactly counter-balance the classical potential force. In essence, the particles would remain fixed in their spatial positions.

In the case of the quantum harmonic oscillator, the quantum trajectories computed using the MWLS procedure agree with the exact analytical results one can obtain for this system. Furthermore, the procedure appears to be stable for long periods of time. We have carried out calculations up to 10 oscillation periods without considerable accumulation of error. We now move on to the more formidable problem of tunneling in a double well potential.

## B. Quantum Tunneling in a Double Well Potential

Tunneling and barrier penetration represent phenomena which are unique to quantum mechanics. It is well understood from classical mechanics that if a particle lacks sufficient energy to surmount a potential barrier, the particle will be reflected and the barrier is impenetrable. However in quantum mechanics, a particle can "pass through" a barrier. This can be rationalized in a variety of ways. Perhaps the most consistent is that if the particle is brought to a halt at the classical turning point, both its position and momentum are defined to exact precision, which would violate the uncertainty principle. In the quantum trajectory approach, the quantum potential acts to enforce this behavior by effectively "lowering" the barrier to permit trajectories to penetrate through the barrier and raises the barrier once sufficient amplitude has passed. To see how this comes about in the context of a particle based approach, let us consider tunneling through the double well potential:

$$V(x) = ax^4 - bx^2 \quad (32)$$

In this example, we take  $a = 0.007$  and  $b = 0.01$  in atomic units, which gives two tunneling states below the barrier at  $E = -369.827\text{cm}^{-1}$  and  $-313.918\text{cm}^{-1}$  and a barrier height of  $V_b = 786.24\text{cm}^{-1}$ . The initial Gaussian density was centered about the center of the right side well at  $x_o = \sqrt{b/2a}$  with  $\beta = \sqrt{4bm}$  corresponding to a harmonic approximation to a state localized in the right hand well. In the lower frame of Fig. 2 we show quantum trajectories for the initial crossing of the wavefunction from the right to the left side of the well and in Fig. 3 we show snapshots of the quantum density, the quantum potential,  $V + Q$ , and  $V(x)$  for various times. The trajectories cross from  $+x$  to  $-x$  corresponding to top to bottom in Fig 2. The initial expansion of the paths is primarily due to the expansion of the wavefunction in the well. Since the initial state is not in a stationary state of the potential, there is a net force on the particles due to the difference between the  $Q'$  and  $V'$ . Once the particles have passed through the barrier region (at  $x = 0$ ), they encounter the repulsive potential wall and are reflected. Note that the particles penetrate fairly deeply into the repulsive region. However, they carry very little net density. Unfortunately as far as our calculations are concerned, we run into numerical difficulties in computing the quantum potential in this region. As a result, the congruency condition fails to hold and trajectories begin to cross (after  $t = 650$ ) and our results are meaningless beyond this point.

However, prior to this point in time, we can compute the effective barrier height due to the quantum potential at  $x = 0$ . In Fig. 4 we plot the effective barrier height,  $V_{eff} = Q(0) + V_b$ , as a function of time. As indicated above, the quantum potential from the initial Gaussian distribution effectively "lowers" the barrier allowing trajectories to pass from the right to the left. However, once the initial expansion of the density is accomplished, the barrier begins to rise and the effective barrier height appears to approach an asymptotic value.

If we assume that the lowest two eigenstates of the double well can be approximated as symmetric and antisymmetric linear combinations of ground state harmonic oscillators centered about the left and right minima in the well, we can compute the approximate quantum potential at  $x = 0$  quite easily. Let us write the approximate wavefunction as (neglecting a common phase factor),

$$\psi(x, t) = \frac{1}{\sqrt{2}}(e^{-i\omega t}\phi_+(x) + e^{+i\omega t}\phi_-(x)), \quad (33)$$

where  $\phi_{\pm}(x)$  are the symmetric and anti-symmetric tunneling states split by  $\hbar\omega = (E_- - E_+)/2$ . Taking,

$$\phi_{\pm}(x) \approx \frac{1}{\sqrt{2}}(\phi_R(x) \pm \phi_L(x)), \quad (34)$$

and using the approximation

$$\phi_{R,L}(x) = \left(\frac{m\omega}{\pi\hbar}\right)^{1/4} e^{-m\omega_o(x \pm x_o)^2/2\hbar}, \quad (35)$$

the quantum potential at the barrier is given by

$$Q(0) = \left(\frac{\hbar\omega_o}{2} + \frac{1}{4}m\omega_o^2 x_o^2(\cos(4t\omega) - 3)\right) \quad (36)$$

Thus, the effective barrier separating the right and left sides of the system is at its minimum when  $\rho$  is localized in the right or left hand well and greatest when  $\rho$  delocalized in a 50:50 mixture of right and left hand states. Moreover, as the separation between the respective wells increases, the harmonic oscillator approximation to the lowest eigenstates becomes better and better. Correspondingly, the quantum potential becomes the parabola,

$$Q(x) \approx \frac{\hbar\omega_o}{2} - \frac{1}{2}m\omega_o^2(x \pm x_o)^2. \quad (37)$$

Since the quantum force and the classical potential force will be nearly equal and opposite, the particles will remain almost motionless in the initial well.

## V. PILOT WAVE TRAJECTORIES

As noted above, the trajectories themselves can be obtained by propagating a solution to the time-dependent Schrödinger equation. In this “pilot wave” scheme, the quantum potential and equations of motion for the Bohmian particles may be computed directly from the wave function itself. Alternatively, if we have an accurate representation of  $\psi$  and can compute  $v[\psi]$  via Eq. 1, we can obtain what should be a set of “exact” Bohmian trajectories associated with the quantum wavefunction. To compute such trajectories for the double well example shown above, we used a discrete variable representation<sup>25</sup> (DVR) of Gauss-Tchebychev quadrature points to represent both the wave packet and the time-evolution operator on a finite spatial grid of 200 quadrature points spanning 2.5 Bohr on either side of the barrier. For dynamics at low total energy, this representation is certainly more than adequate as we were able to converge the lowest 20 eigenstates of this well to  $1 : 10^6$ . Because the instantaneous position of a Bohmian particle at  $x(t)$  will not generally correspond to the position of a quadrature point, the velocity can not be computed directly from the DVR wavefunction, which is only defined on the quadrature points themselves. Rather, we transform  $\psi$  from the DVR to a finite basis representation (FBR) using the unitary transformation,

$$\psi^{FBR} = U \cdot \psi^{DVR}, \quad (38)$$

where  $U$  is the unitary transformation associated with a  $N$ -point Gauss-Tchebychev DVR.

$$U_{ij} = \sqrt{\frac{2}{N+1}} \sin\left(ij \frac{\pi}{N+1}\right). \quad (39)$$

The elements of the vector  $\psi^{FBR}$  are the expansion coefficients of the wavefunction in a finite polynomial basis.

$$\psi(x, t) = \sum_{i=1}^n \psi_i^{FBR}(t) T_i(x). \quad (40)$$

For the Gauss-Tchebychev quadrature scheme used here, basis functions are:

$$T_i(x) = \sqrt{\frac{2}{\Delta}} \sin(i\pi(x - \Delta/2)/\Delta). \quad (41)$$

Eq. 37 gives the wavefunction at any point  $x \in [-\Delta/2, \Delta/2]$  and we can use this information to compute the velocity of a particle guided by  $\psi$ . In the top frame of Fig. 2 we show the Bohm trajectories for the double well system choosing identical conditions as above, this time computed via the DVR pilot wave based procedure. For clarity we show only those trajectories for particles starting to the left of the initial centroid of the density. At long times, the trajectories transmitted to the left hand well tend to bunch together. This is due to the fact that the finite basis functions in Eq. 38 go to zero at  $x = \pm\Delta/2$  and force the system to have an artificial node at the boundary points. Consequently, the quantum potential is infinitely repulsive at the end of the grid and all particle trajectories are repelled from these regions. For practical purposes, the density carried by these trajectories is negligible and the overall effect on the wavepacket dynamics is minimal.

Notice, however, that between  $t = 600$  and  $t = 800$ , a number of trajectories near the barrier at  $x = 0$  are deflected from each other. This is due to the fact that  $\rho$  develops oscillatory structure due to constructive and destructive interferences between on coming and reflected components of the wavefunction near the barrier. The density eventually develops a node at about  $t = 900$  a.u. Surprisingly, and disturbingly, this behavior is absent in the MWLS trajectories. In Figure 5 and Figure 6 we compare the evolution of  $\rho$  using the DVR ( $\rho^{DVR}$ ) and MWLS ( $\rho^{MWLS}$ ) methods. Initially, the agreement is quite good. At longer times the agreement is very poor with  $\rho^{MWLS}$  even “looping back” through itself. At intermediate times, as  $\rho$  is reflected by the repulsive barrier in the  $-x$  half of the double well, oscillations develop in  $\rho^{DVR}$  whereas no such oscillations are seen in  $\rho^{MWLS}$ . Since the quantum potential is a measure of the local curvature of  $\rho$ , these oscillations translate into attractive and repulsive regions in the quantum potential. Eventually as  $\rho^{DVR}$  goes on to form nodes (at approximately  $t = 700$  au and 900 au

trajectories are guided away from such regions via the quantum force. This accounts for the significant deflections in the DVR trajectories but does not tell us why this fails to occur in the MWLS case.

The answer is basically that of sampling resolution. As the MWLS trajectories evolve, they by in large tend to spread apart. This restricts our ability to resolve any structure in  $\rho^{MWLS}$  which occurs on lengthscales finer than the distance of separation of the MWLS trajectories at a given point in time. Hence, the oscillatory structure seen in the DVR calculations (e.g. at  $t=550$  au) are too fine to be resolved by the MWLS trajectories. Thus, the quantum potential will be too smooth in this region. The DVR calculations are also band width limited due to the finite spacing of the DVR points. However, in the DVR grid used in these examples, this spacing is fixed at  $\delta x = 0.049$  Bohr, where as in the MWLS case the spacing between trajectories in the region of the barrier at  $t = 550$  is  $\approx 0.10$  Bohr, which slightly courser than the structure seen in  $\rho^{DVR}$  in this region. Consequently, the MWLS trajectories lose band width resolution precisely where it is needed the most in this case.

Let us compare the DVR and MWLS based trajectories on a head to head basis. Four sets of trajectories extracted from Fig. 2 are shown in Figure 7. First, for trajectories originating near the leading edge of the MWLS grid, we expect that the two results should deviate rather early due to the fact that the fitting procedure used to compute the quantum potential using the MWLS is least accurate near the end of the grid (Trajectory # 9). Surprisingly, however, the agreement is quite good. In fact, it is apparent that the deviation is more likely due to the artificial boundary conditions imposed by the basis function used to represent the quantum wave packet in the DVR calculations. For trajectories originating near the maximum of the initial wavepacket (Trajectory #50), we see quantative agreement between DVR and MWLS based trajectories since  $\rho$  is smooth function of  $x$  in this region and remains so over the course of both calculations. However, let us compare the two trajectories labeled #38 and #39 from each calculation. These two trajectories originate side by side separated by  $\delta x = 0.02 \text{ Bohr}$ . In the DVR calculation, these trajectories are deflected by the oscillations in  $\rho$  with #38 deflected slightly towards the  $-x$  direction and #39 in the  $+x$  direction. These deflections are not observed in the corresponding MWLS trajectories.

## VI. DISCUSSION

In this paper, we present our implementation and computational analysis of the de Broglie-Bohm hydrodynamic equations using a particle based description. The formalism itself allows an elegant interpretation of quantum dynamics in geometric terms. Instead of wave functions, we have geometric ray lines. Surprisingly, this intuitive connection between quantum wave mechanics and geometry has not made it into the “main stream” even though the original seeds for this interpretation can be found at the very advent of quantum theory. However, we do note that this view point is seeing a resurgence in popularity as measured by the number of papers which have used the Bohmian construction in vastly different areas of quantum physics.

What is important, however, to point out that we are only showing the best case scenarios in this paper. We have found that trajectories tend to cross cases in which  $\rho$  is very small, trajectory lines are far apart, or when the potential is significantly anharmonic. Some of this is exhibited in Figures 2 and 3. This is most certainly a result of numerical instabilities in the MWLS procedure which we have elaborated upon in this paper.

We also run into particular difficulties in dealing with nodal points in the density, in other words, when  $\rho(x) = |\psi(x)|^2 = 0$ . At such points, it is not possible to fit the coefficients of a polynomial expansion using points on either side of the node since the function does not have continuous derivatives at the node. We have tried various computational alternatives to dealing with such points. One alternative is to use only trajectories and densities on one side of the node or the other when computing  $Q(x)$ . Under this approach we compute derivatives by approaching the node from the right and from the left. Another alternative we have tried is to introduce a  $\log(x - x_n)$  basis function for stars which include nodal points. Both of these approaches give very good results for cases in which the initial wavefunction was taken as an odd parity eigenstate in a symmetric well. However, both cases require prior knowledge of the location of the node and that parity be a constant of the motion so that the node does not move. For cases in which parity is not a constant of the motion, nodal points can occur over the natural course of the evolution of the quantum wavefunction, even if the initial wavefunction has no nodes initially. We speculate that a solution may be to construct

$$R_i = \sqrt{\rho_i} e^{i\mu\pi} \quad (42)$$

along each  $x_i(t)$  trajectory where  $\mu = 0, 1, 2, \dots$  accounts for the branch cut taken when evaluating  $\sqrt{\rho}$  on either side of a node.<sup>26</sup> In essence, on one side of a node  $R > 0$  and  $\mu = 0, 2, \dots$ , while on the other side,  $R < 0$  and  $\mu = 1, 3, \dots$ . This would preserve analyticity across the node allowing us to calculate  $Q$  using a simple polynomial basis. At present, the treatment of nodes and their evolution is an open problem which we will take up in a future work.<sup>27</sup>



## ACKNOWLEDGMENTS

This work was supported by grants from the Robert A. Welch Foundation and the National Science Foundation. The author also wishes to thank Prof. Bob Wyatt (Univ. of Texas), Prof. Don Kouri (U. Houston) and Dr. Pablo Yepes (Rice) for stimulating discussions.

- 
- <sup>1</sup> L. de Broglie, in *Reports on the Solvay Congress*, Gauthers-Villars et Cie., Paris, 1928.
  - <sup>2</sup> L. de Broglie, *Compt. Rend. Acad. Sci. Paris* **183**, 447 (1926).
  - <sup>3</sup> L. de Broglie, *Selected papers on wave mechanics* (Blackie, London, 1928).
  - <sup>4</sup> L. de Broglie, *An introduction to the study of wave mechanics*, (E. P. Dutton and Company, New York, 1930).
  - <sup>5</sup> L. de Broglie, *Théorie de la Quantification dans la nouvelle mécanique* (Georges Thone, Liège, 1932).
  - <sup>6</sup> E. Madelung, *Z. Phys.* **40**, 322 (1929).
  - <sup>7</sup> D. Bohm, *Phys. Rev.* **85**, 166 (1952).
  - <sup>8</sup> D. Bohm, *Phys. Rev.* **84**, 180 (1952).
  - <sup>9</sup> P. R. Holland, *The quantum theory of motion*, (Cambridge Univ. Press, 1993).
  - <sup>10</sup> J. H. Weiner and Y. Partom, *Phys. Rev.* **187**, 1134 (1969).
  - <sup>11</sup> J. H. Weiner and A. Askar, *J. Chem. Phys.* **54**, 1108 (1971).
  - <sup>12</sup> A. Askar and J. H. Weiner, *Am. J. Phys.* **39**, 1230 (1971).
  - <sup>13</sup> A. Askar and M. Demiralp, *J. Chem. Phys.* **60**, 2762 (1974),
  - <sup>14</sup> B. K. Day, A. Askar, and H. A. Rabitz *J. Chem. Phys.* **109**, 8770 (1998).
  - <sup>15</sup> F. S. Mayor, A. Askar, and H. A. Rabitz, *J. Chem. Phys.* **111**, 2423 (1999).
  - <sup>16</sup> C. L. Lopreore and R. E. Wyatt, *Phys. Rev. Lett.* **82**, 5190 (1999).
  - <sup>17</sup> R. E. Wyatt, *Chem. Phys. Lett.* **313**, 189 (1999).
  - <sup>18</sup> R. E. Wyatt, *J. Chem. Phys.* **111**, 4406 (1999).
  - <sup>19</sup> W. H. Press, S. A. Teukolski, W. T. Vetterling, and B. P. Flannery, *Numerical Recipes in C, 2nd Ed.*, (Cambridge Univ. Press, England, 1992).
  - <sup>20</sup> T. J. Liszka, C. A. M. Duarte, and W. W. Tworzydło, *Comput. Methods Appl. Mech. Engrg.* **139**, 263 (1996).
  - <sup>21</sup> B. Jaing, *The Least Squares Finite Element Method*, (Springer-Verlag, Heidelberg, 1998).
  - <sup>22</sup> R. Aris, *Vectors, tensors, and the basic equations of fluid mechanics* (Prentice-Hall, Englewood Cliffs, New Jersey, 1962).
  - <sup>23</sup> B. Schutz, *Geometric Methods of Mathematical Physics* (Cambridge Univ. Press, Cambridge, UK, 1995).
  - <sup>24</sup> L. Verlet, *Phys. Rev.* **159**, 98 (1967); *Phys. Rev.* **165**, 201 (1968).
  - <sup>25</sup> J. C. Light, I. P. Hamilton, and J. V. Lill, *J. Chem. Phys.* **85**, 1400 (1985).
  - <sup>26</sup> Similar thoughts along these lines regarding the "node" problem are presented in Ref. 16.
  - <sup>27</sup> E. R. Bittner and R. E. Wyatt, manuscript in preparation.

FIG. 1. Quantum trajectories for harmonic oscillators. In each case, the oscillation period,  $\tau = 2\pi/\omega = 888.57au$ . In cases A & D,  $m = 2000au$  while in case B,  $m = 200au$ . Case D is a set of classical trajectories ( $Q = 0$ ) for this system.

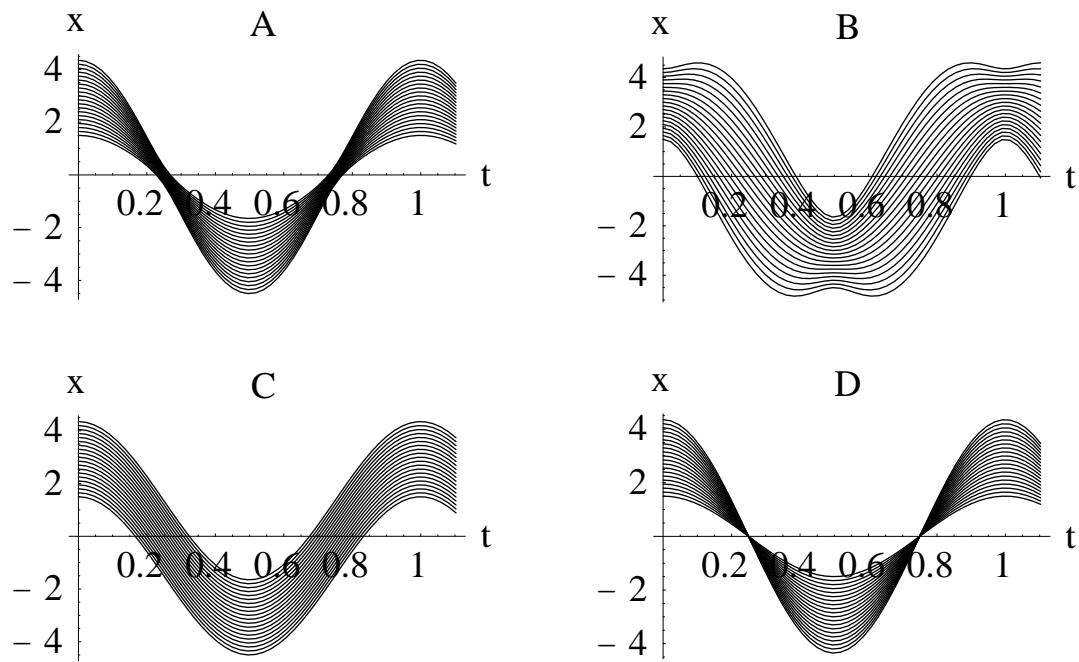


FIG. 2. Bohmian trajectories computed via wavepacket propagation (DVR) versus particle based trajectory method (MWLS).

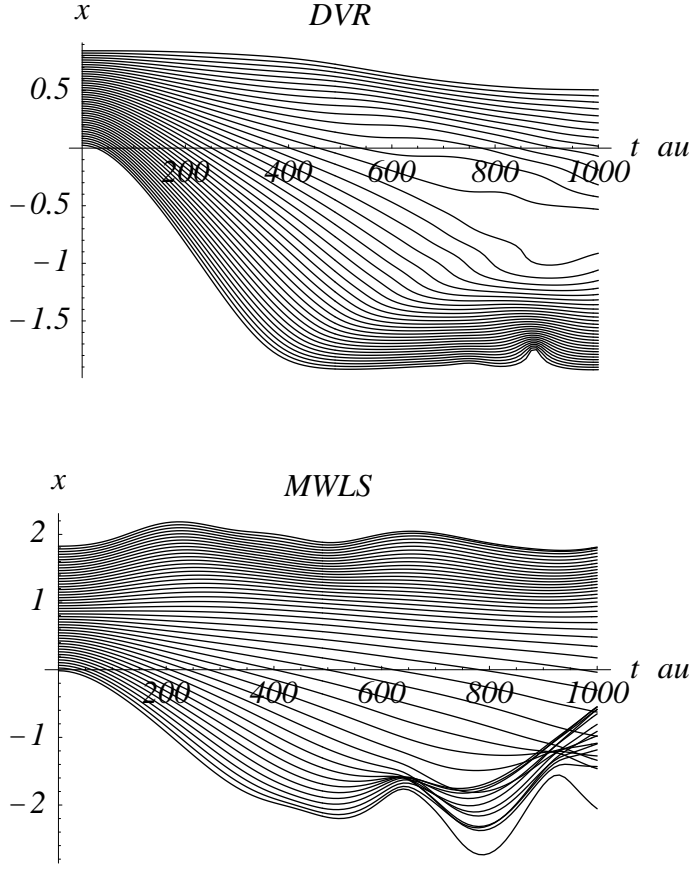


FIG. 3. Evolution of quantum density,  $\rho$  (dots), quantum potential (short dashed lines),  $V(x)$  (solid line), and  $V + Q$  (long dashed lines) for a proton in a double well potential at various times.

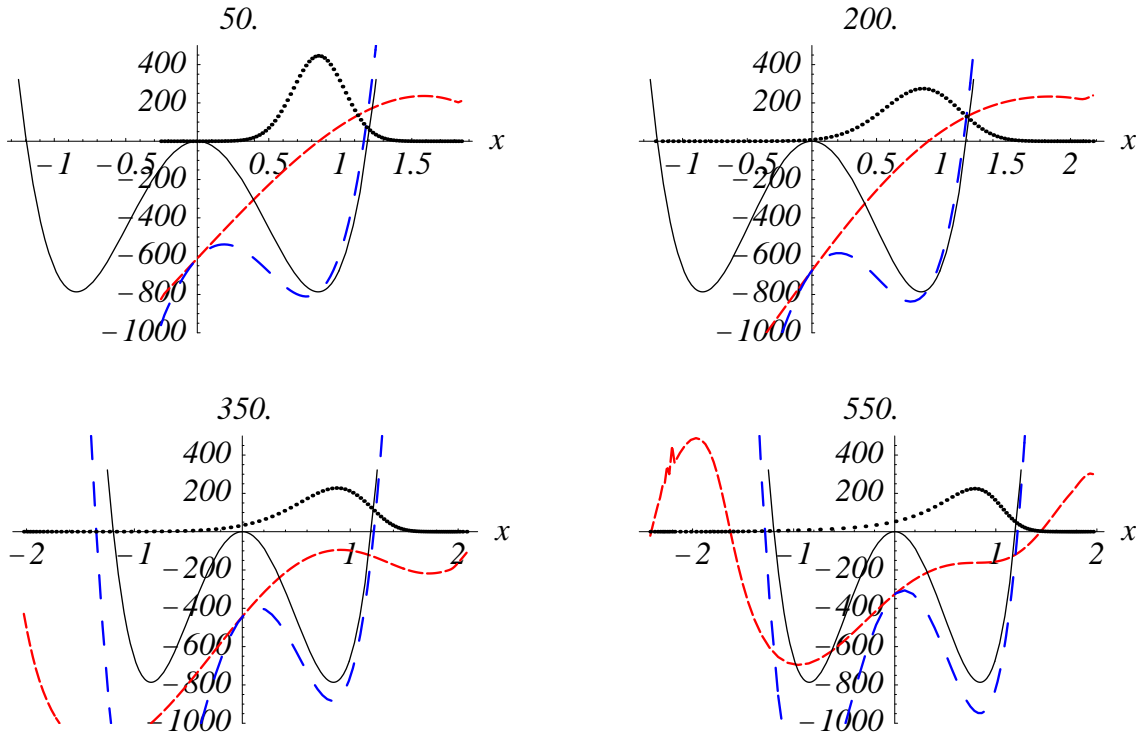


FIG. 4. Effective barrier relative to bottom of well encountered by quantum trajectories in the double well problem in crossing from right to left hand well.

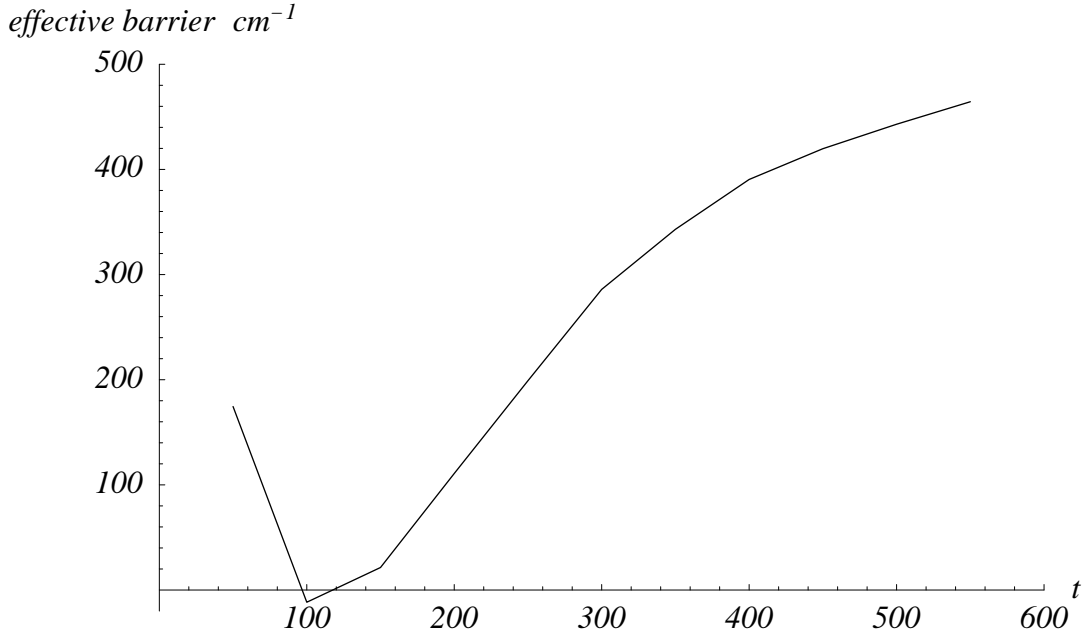


FIG. 5. Evolution of the quantum density,  $\rho$ , as computed via MWLS based methods.

# *MWLS calculation*

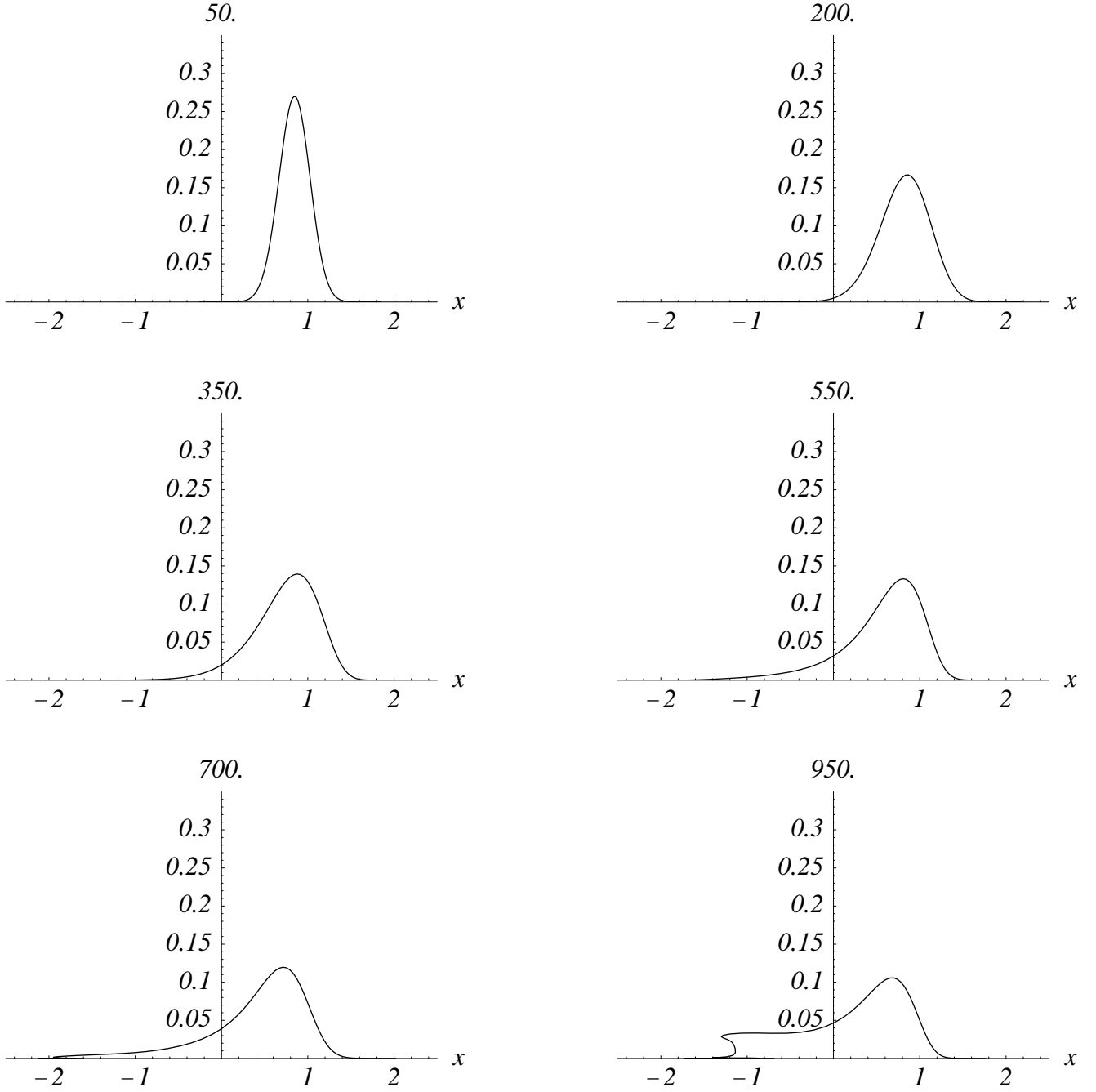


FIG. 6. Evolution of the quantum density,  $\rho$ , as computed via DVR based methods. Note in particular the interference structure which develops in the DVR calculation which does not appear in the MWLS trajectory calculations shown in Figure 5.

# DVR calculations

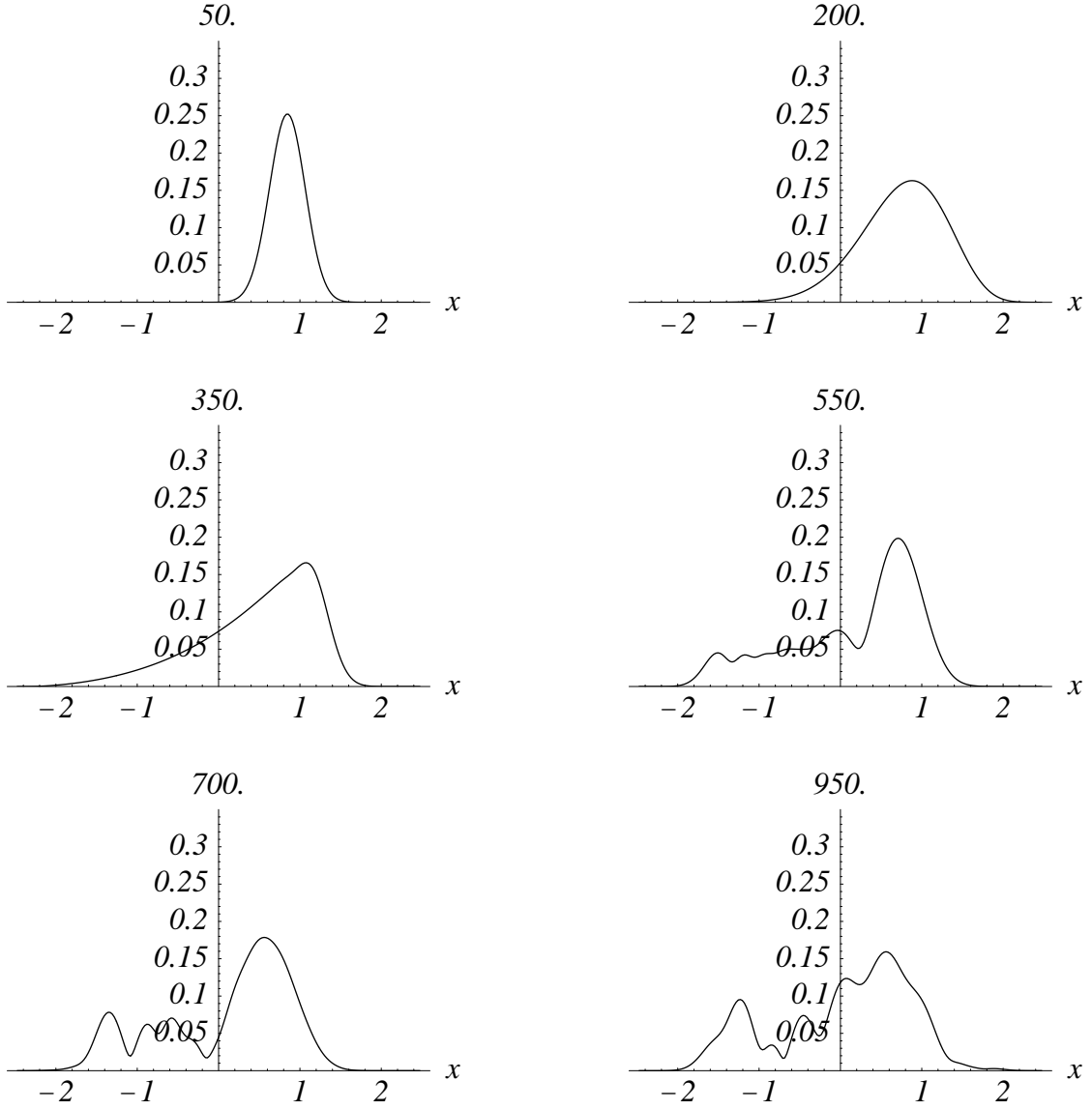


FIG. 7. Comparison of 4 trajectories computed via DVR (dashed) versus MWLS (solid) methods.

